9. Murthy, D. S. N., Dayal, A. M., Natarajan, R., Balaram, V. and Govil, P. K., *J. Geol. Soc. India*, 1997, **49**, 123–132.

10. Chalapathi Rao, N. V., Ph D thesis, Cambridge University, 1997.

11. Hanson, G. N., *Annu. Rev. Earth Planet. Sci.*, 1980, **8**, 371–406.

12. Hanson, G. N., *Rev. Mineral.*, 1989, **21**, 79–97.

13. Shaw, G. M., *Geochim. Cosmochim. Acta*, 1970, **34**, 237–243.

14. McKenzie, D., *J. Petrol.*, 1984, **25**, 713–765.

15. Watson, E. B., Brenan, J. M. and Baker, D. R., in *Continental Mantle* (ed. Menzies, M. A.), Oxford Monographs on Geology and Geophysics, London, 1990, vol. 16, pp. 111–122.

16. Harte, B., Hunter, R. H. and Kinny, P. D., *Philos. Trans. R. Soc. London*, 1993, **A342**, 1–21.

17. McKenzie, D. and O'Nions, R. K., *J. Petrol.*, 1991, **32**, 1021–1091.

18. Parkar, R. L., *Annu. Rev. Earth Planet. Sci.*, 1977, **5**, 35–64.

19. McKenzie, D. and O'Nions, R. K., *J. Petrol.*, 1995, **36**, 133–159.

20. Nixon, P. H., Rogers, N. W., Gibson, I. L. and Grey, A., *Annu. Rev. Earth Planet Sci.*, 1981, **9**, 285–309.

21. Richardson, S. H., Erlank, A. J. and Hart, S. R., *Earth Planet. Sci. Lett.*, 1985, **75**, 116–128.

22. Boyd, F. R., *Earth Planet. Sci. Lett.*, 1989, **96**, 15–26.

23. Boyd, F. R., Pearson, D. G., Nixon, P. H. and Mertzman, S. A., *Contrib. Mineral. Petrol.*, 1993, **113**, 352–366.

24. Schulze, D. J., *J. Geophys. Res.*, 1995, **100**, 12513–12526.

25. Ganguly, J. and Bhattacharya, P. K., in *Mantle Xenoliths* (ed. Nixon, P. H.), John Wiley and Sons Ltd, New York, 1987, pp. 249–266.

26. Nehru, C. E. and Reddy, T. A. K., *Geol. Soc. Austral. Spec. Publ.*, 1989, **14**, 745–758.

27. Piper, J. D. A., *Earth Planet. Sci. Lett.*, 1982, **59**, 61–89.

28. Windley, B. F., in *The Evolving Continents*, John Wiley and Sons, New York, 1995, pp. 526.

29. Erlank, A. J., Waters, F. G., Hawkesworth, C. J., Haggerty, S. E., Allsopp, H. L., Rickard, R. S. and Menzies, M. A., in *Mantle Metasomatism* (eds Menzies, M. A. and Hawkesworth, C. J.), Academic Press, London, 1987, pp. 221–311.

30. Hawkesworth, C. J., Fraser, K. J. and Rogers, N. W., *Trans. Geol. Soc. S. Afr.*, 1985, **88**, 439–447.

31. Fraser, K. J., Hawkesworth, C. J., Erlank, A. J., Mitchell, R. H. and Scott-Smith, B. H., *Earth Planet. Sci. Lett.*, 1985, **76**, 57–70.

32. McKenzie, D., *Earth Planet. Sci. Lett.*, 1989, **95**, 53–72.

33. Kramers, J. D., Smith, C. B., Lock, N. P., Harmon, R. S. and Boyd, F. R., *Nature*, 1981, **291**, 53–56.

34. Richardson-Bunbury, J. M., Ph D thesis, Cambridge University, 1992, pp. 185.

35. Rajamani, V., Shiv Kumar, K., Hanson, G. N. and Shirey, S. B., *J. Petrol.*, 1985, **96**, 92–123.

36. Rajamani, V., Shirey, S. B. and Hanson, G. N., *J. Geol.*, 1989, **79**, 487–501.

37. Balakrishnan, S., Rajamani, V. and Hanson, G. N., *Contrib. Mineral. Petrol.*, 1989, **107**, 279–292.

38. Mallikharjuna Rao, J., Bhattacharjee, S., Rao, M. N. and Hermes, O. D., *Geol. Soc. India Mem.*, 1995, **33**, 307–328.

Estimation of tectonic stress in NW Himalaya region using IRS-1B data

Pradeep K. Sahoo, Sandeep Kumar and Ramesh P. Singh*

Department of Civil Engineering, Indian Institute of Technology, Kanpur 208 016, India

Earthquake records, landslide and recent changes in geomorphological features indicate that area between Main Boundary Thrust (MBT) and Main Frontal Thrust (MFT) is tectonically active. Spectral and spatial enhancement techniques have been employed for the digital data of IRS-1B LISS-I to delineate the lineaments and major faults of the area. Based on Mohr's theory failure criteria and statistical analysis of remotely sensed lineament data, the horizontal compressive stress (S_{Hmax}) has been estimated at various sites of the study area. These data are found to be consistent with the published S_{Hmax} orientation determined from earthquake focal mechanism solution.

SATELLITE remote sensing has emerged as a powerful tool for seismic hazard assessment and mapping[1-3]. The synoptic overview of a wide area and digital nature of the remote sensing data can be utilized suitably to map the active tectonic features. In the present study, the area around Dehradun lying between the lat. 29.52°–31.18°N and long. 76.89°–78.55°E (Figure 1), NW Himalaya, has been chosen for the study of the present tectonic stress using remote sensing data. This area is part of the active tectonic zone of the Indian and Eurasian plate collision 40 million years ago. This area has experienced devastating earthquakes like Kangra (1905) and Uttarkashi (1991) due to the recent earth movements or stress deformations. Analyses of the catalogue of past earthquakes have revealed that these earthquakes are not isolated events, but only the latest expression of diffuse seismic activities.

We have taken IRS-1B LISS-I digital data covering path 29 and rows 46 of October 20, 1994 for detailed analysis. The data consists of 2500 rows and 2350 columns. The whole scene shown in Figure 2 is divided into 19 windows of size 512×512 pixels depending upon the morphology of the area. We have made efforts to enhance the edges using numerous filters in horizontal, vertical and two diagonal directions. For mapping of

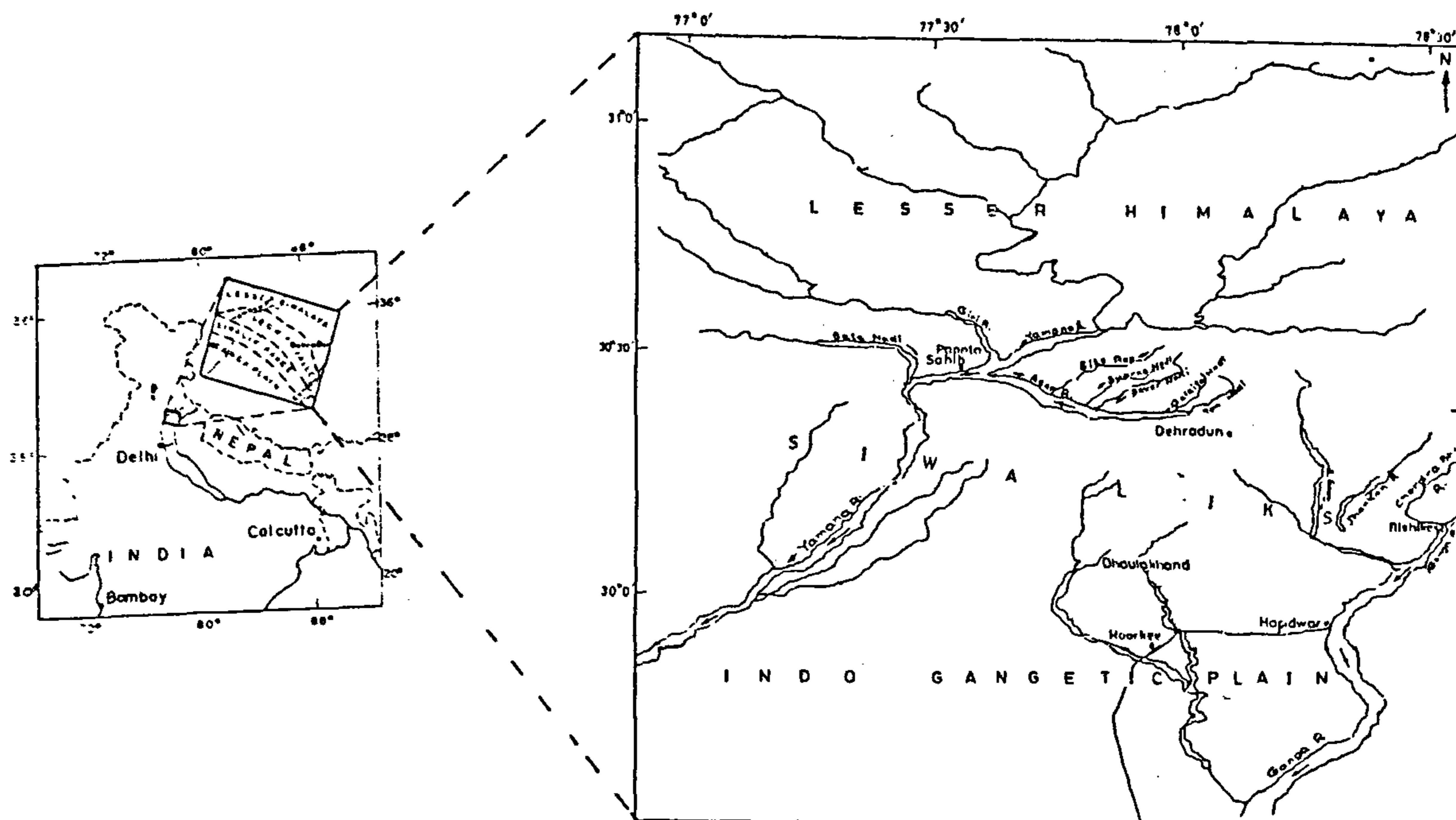*For correspondence. (e-mail: ramesh@iitk.ernet.in)

Figure 1. Location map of the study area.

the horizontal edges in an image, we have used the following 3×3 filter

$$\begin{vmatrix} 1 & 1 & 1 \\ 0 & 0 & 0 \\ -1 & -1 & -1 \end{vmatrix}$$

Horizontal

The above filter computes a value for the central pixel under the template that is accumulated difference vertically between pixels on three rows spaced two apart. Filters used for detecting edges in vertical and two diagonal directions are given as:

$$\begin{vmatrix} 1 & 0 & -1 \\ 1 & 0 & -1 \\ 1 & 0 & -1 \end{vmatrix} \quad \begin{vmatrix} 1 & 1 & 0 \\ 1 & 0 & -1 \\ 0 & -1 & -1 \end{vmatrix} \quad \begin{vmatrix} 0 & 1 & 1 \\ -1 & 0 & 1 \\ -1 & -1 & 0 \end{vmatrix}$$

Vertical Diagonal Diagonal

All four 3×3 kernels have been used to detect existing edges in all directions. This requires four passes over image data and four separate images have been prepared for each window showing edges in all four directions. As these filters detect only the edges with a background zero value pixels, it is difficult to interpret the resulting filtered images. Consequently, if the edge detection filtered image is subtracted from the smoothed image,

the resultant difference image enhances the edges in a smoothed background. Generally, in band 4 (infrared) we have found large variation of pixel values along the dislocations, faults, fractures and stream valleys in hilly terrain. The edge detection filters assigned maximum pixel values along these lines, due to this maximum reflectance is seen after subtracting the edge detected image from the smoothed image of the area specially in the infrared band.

Lineaments have been mapped by visual interpretation of FCC images and edge enhancement techniques. Visual interpretation has been carried out based on lithological dislocations, joints and fracture traces, truncation of outcrops, alignment of streams, sudden bending of stream etc. Enhanced edges have been considered which are related to difference in vegetation, micro-fractures, joints, fault scarps, slopes, etc. The edges reflect the micro-lineament patterns of the area, which have been mapped suitably by on-screen digitization of the edges using ERDAS software package. All possible lineaments have been digitized on the screen from the edge-enhanced images in four directions, eg. vertical, horizontal and two diagonal directions. Finally, they have been merged with the visually interpreted lineaments in order to get total lineament pattern of the area (Figure 3 a). The latitude and longitude of initial and final points of each lineament have been stored during digitization process for their further statistical treatment.

782

Figure 2. Image of NW Himalayan region.

A computer program has been developed to plot the rose diagram of remotely sensed lineament fabric and estimation of the maximum horizontal compressive stress (S_{Hmax}). The algorithm to plot the rose diagram is based on the basic concept of rose diagram. The latitude and longitude values of initial and final points of each lineament have been taken as input from the ERDAS digitized file and the slope of the lines has been calculated using the following formula:

$$\text{slope} = \frac{(\text{lt}_f - \text{lt}_i)}{(\text{ln}_f - \text{ln}_i)}, \tag{1}$$

where, ln_i, and lt_i are the longitude and latitude of initial point of the lineament, respectively, and ln_f and lt_f are the longitude and latitude value of the final point of the lineament, respectively.

The slope of each lineament has been calculated by the above procedure and grouped into classes for a particular class interval (10°) from the north to plot the rose diagram of the lineament data. Here the radius of rose diagram for particular class is equal to the square root of number of lineaments in that class. Similar procedures have been followed for all selected windows, and rose diagrams have been plotted. Finally, the rose diagrams of all windows are mosaic in one plane fixing the center of each rose diagram in the central longitude and latitude of their corresponding windows (Figure 3 b).

Rose diagram of lineament fabric reveals that there is a distinct change in major trend of lineament in north and south of MBT. In the Lesser Himalayan region, maximum number of lineaments are oriented in east–west direction (N80°–90°E). In Dun and Siwalik region, the trend of majority of lineaments are found to be in the direction of N40°–50°E.

The orientation of fault planes are primarily controlled by the direction of principal stress. Thus, the principal stress direction σ_1 can be determined from the orientation of fault plane. Quantification of fault plane orientation with respect to principal stress direction is of paramount

importance in structural analysis. For determination of angle 'θ' between the direction of maximum compressive stress (i.e. the maximum principal stress σ_1, and failure plane direction more accurately, Mohr's theory of failure for granular material is taken into consideration. Based on Mohr's theory of failure, the angle between the failure plane and σ_1 direction is given as[4],

$$\theta = 45 - \phi/2, \tag{1}$$

where θ is angle between failure plane and σ_1 direction, and ϕ is internal frictional angle.

In the present context, most of the lineaments and faults represent slip faces, which have been considered as the result of continued horizontal maximum compressive stress (S_{Hmax}) due to Indian plate movement against Eurasian plate. The direction of stress acted on each element of failure has been estimated using equation (1).

We have estimated the stress direction from the lineament pattern using standard ϕ value of the rocks present in the area. We have taken values[5] of ϕ as 25°, 30° and 33° for Doon gravels, Siwalik sandstone and Lesser Himalayan metamorphics, respectively. The orientation of stress acting on each lineament with respect to north has been calculated and grouped into classes of 10° interval. This procedure has been repeated in each selected window of 512×512 pixel dimension and the results have been plotted as rose diagrams. Finally, each rose diagram is assigned to its appropriate position in the main scene with respect to their positions in terms of longitude and latitude (Figure 4 a). The stress map of the area has been prepared taking the angle of maximum frequency of stress rose diagram as S_{Hmax} orientation (Figure 4 b). The S_{Hmax} orientation at different sites determined by above method is given in Table 1.

The above data shows that average S_{Hmax} direction of all sites of Lesser Himalayan range is N50°–60°E. In Dun valley and Siwalik range average S_{Hmax} orientation is N20°–30°E, except at Yamuna tear fault (site no. 16) and Dhaulakhand fault (site no. 18) area where the orientation is found in the range of N40°–50°E. Lesser


Figure 3 a. Total lineament map of the area.

Table 1. S_{Hmax} orientation at different sites derived from remotely sensed lineament data

Site no.	Longitude	Latitude	Azimuth (from N)	Region
1	77.08	30.95	40–50	Lesser Himalaya
2	77.41	30.95	50–60	
3	77.74	30.95	50–60	
4	78.07	30.95	40–50	
5	78.36	30.95	40–50	
6	77.08	30.68	50–60	
7	77.41	30.68	50–60	
8	77.74	30.68	50–60	
9	78.07	30.68	50–60	
10	78.36	30.68	50–60	
11	78.34	30.35	50–60	
12	78.34	30.42	20–30	Doon Valley
13	77.78	30.37	20–30	
14	77.08	30.42	20–30	Siwaliks
15	77.27	30.42	20–30	
16	77.53	30.42	50–60	
17	77.78	30.42	20–30	
18	78.08	30.17	50–60	
19	78.34	30.02	20–30	

Himalayan rocks are older than Siwaliks and are made up of Precambrian and Palaeozoic rocks. The orientation of average maximum horizontal compressive stress (S_{Hmax}) direction in the Lesser Himalayan region shows the palaeostress direction. The average maximum horizontal compressive stress (S_{Hmax}) direction for the Siwalik region found to be about N20–30°E indicates the contemporaneous maximum horizontal compressive stress orientation in the region. This has also been found by Jain[6] from the interpretation of aerial photographs and Landsat imagery.

Using three different stress indicators, i.e. borehole elongation breakouts, in-situ hydrofracturing measurement and earthquake focal mechanism, Gowd et al.[7] have prepared the maximum horizontal stress (S_{Hmax}) orientation regime of the Indian sub-continent which is incorporated in the world stress map. From the stress[7] map of India, it is found that the maximum horizontal compressive stress in the study area is about N23°E. The estimated stress shows the maximum stress direction within the range varying from N20°E to N30°E in Dun valley and Siwalik region. A fair assumption, that the active stress direction is taken at an interval of 10° instead of a particular value, is authentic as the study
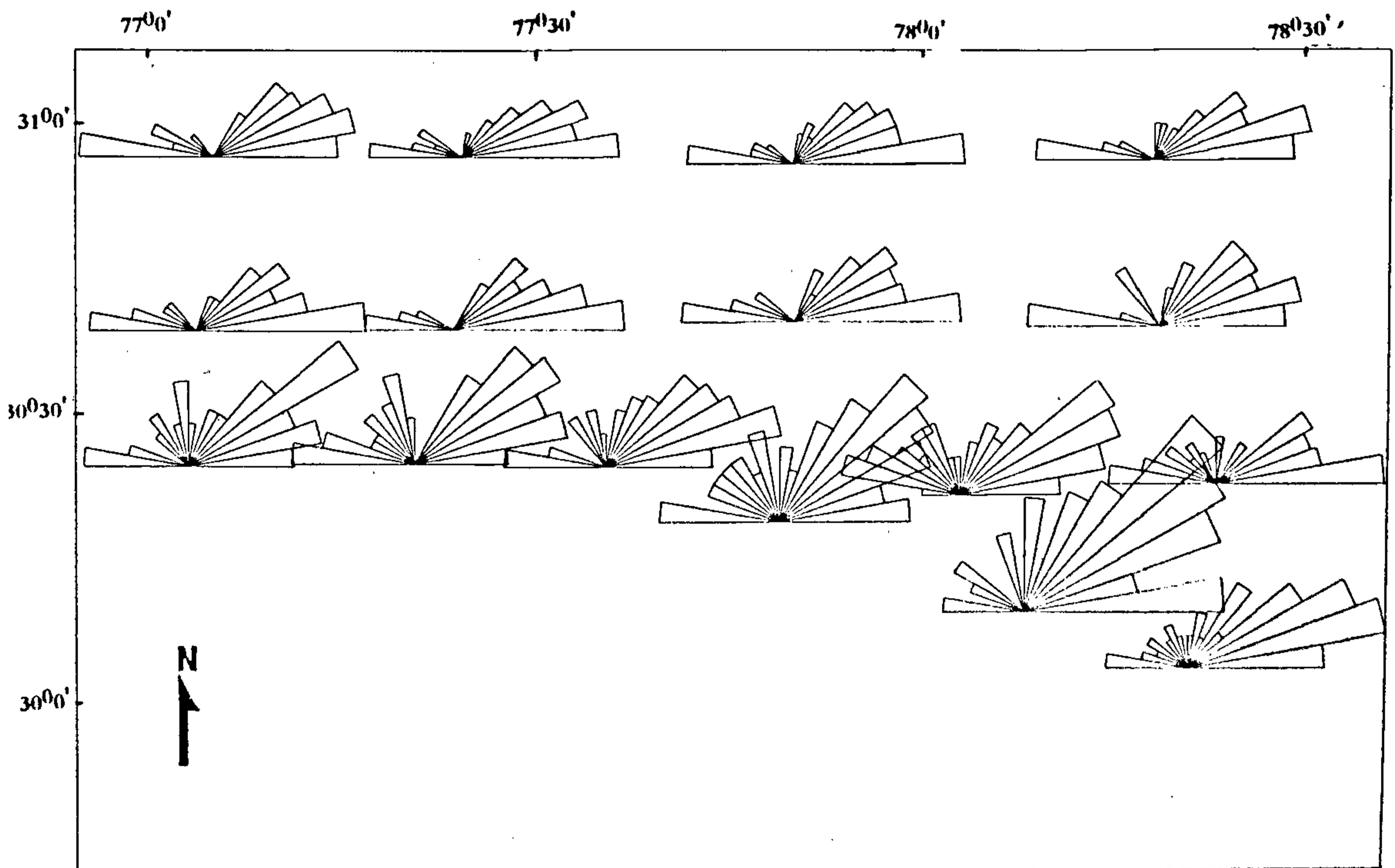
Figure 3 b. Rose diagram showing orientation of lineaments from north at 10° intervals at various locations in the area.
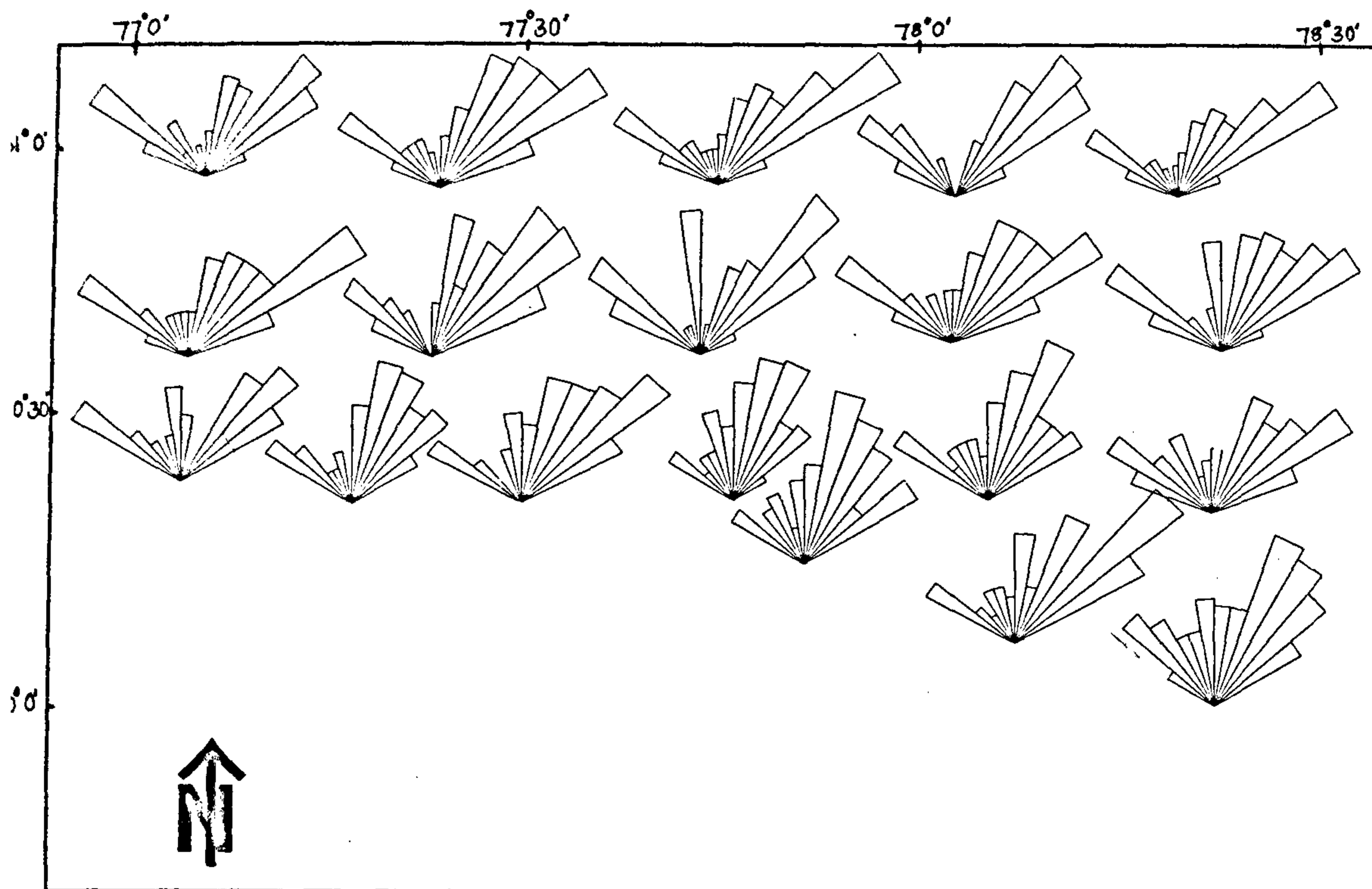
Figure 4 a. Rose diagram showing S_{Hmax} orientation from north at 10° intervals at different sites in the study area.
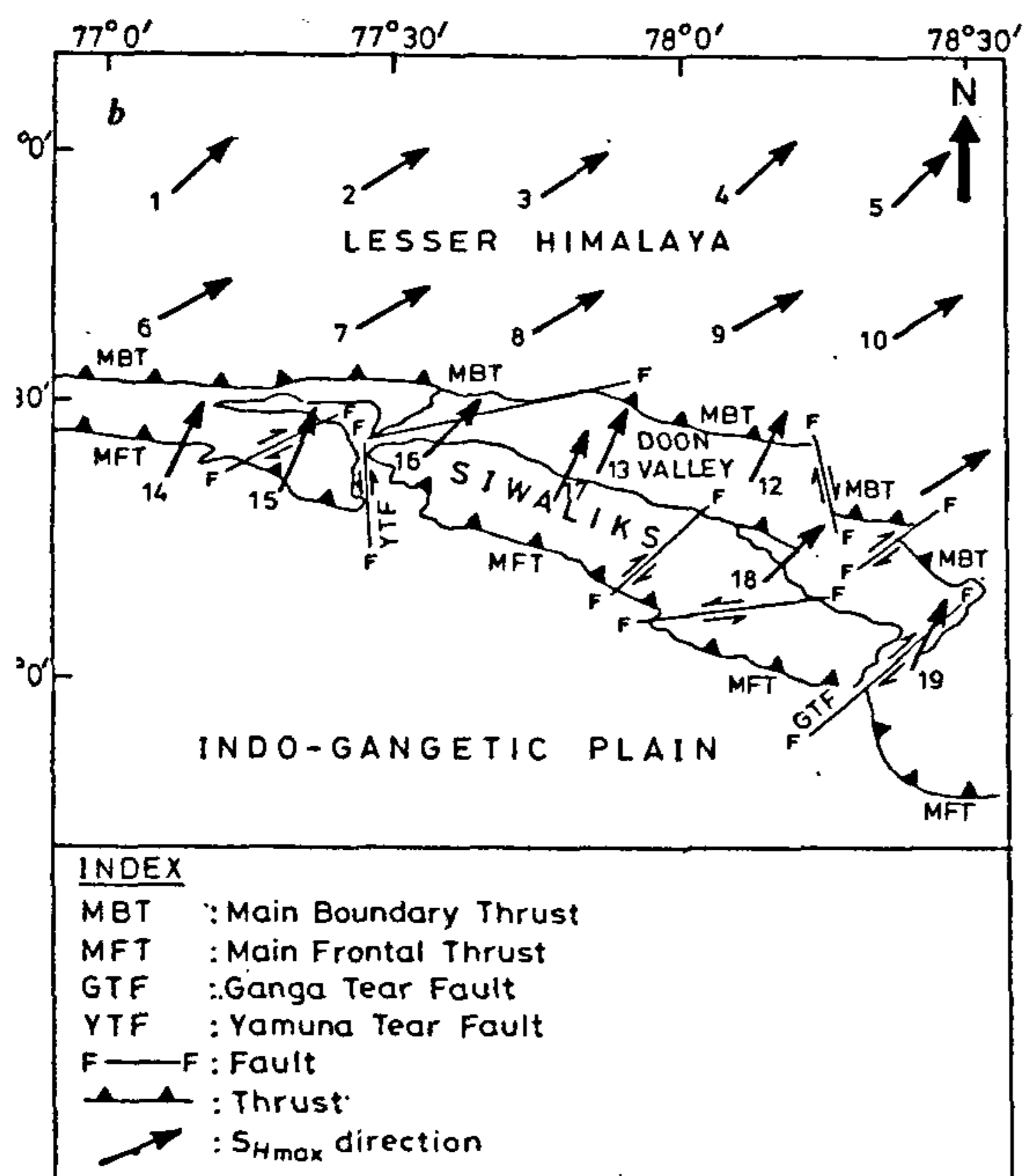

INDEX

MBT	: Main Boundary Thrust
MFT	: Main Frontal Thrust
GTF	: Ganga Tear Fault
YTF	: Yamuna Tear Fault
F——F	: Fault
▲—▲—	: Thrust
⟋	: S_{Hmax} direction

Figure 4 b. Stress map of the area showing S_{Hmax} direction.

area comprises of different rock types of varying ϕ values and other inhomogenity.

It is clear that the Lesser Himalayan region shows palaeostress due to previous orogenies whereas Siwalik region indicates the contemporaneous S_{Hmax}, maximum horizontal stress orientation direction. The present results show that the lineament mapping of Siwalik region using remote sensing data will prove to have paramount importance in understanding the Himalayan orogeny.

1. Cavallin, A. and Marchetti, M., Adv. Space Res., 1995, 15, 45–55.
2. Murphy, W., in Proceedings of Conference of Natural Hazard Assesment and Mitigation: the Unique Role of Remote Sensing, Royal Society, London, U.K., 1994, pp. 7–12.
3. Singhroy, V., Adv. Space Res., 1995, 15, 67–78.
4. Cernica, John N., in Geotechnical Engineering Soil Mechanics, John Wiley and Sons Inc., 1995, pp. 259–271.
5. Hock, E. and Bray, J., Rock Slope Engineering, The Institution of Mining and Metallurgy, London, 1977, pp. 100–101.
6. Jain, A. K., J. Geol. Soc. India, 1987, 30, 169–186.
7. Gowd, T. N., Sriram Rao, S. V. and Gaur, V. K., J. Geophys. Res., 1992, 97, 11,879–11,888.